First Observation of the Decay $B_{s2}^*(5840)^0 \to B^{*+}K^-$ and Studies of Excited B_s^0 Mesons

R. Aaij *et al.*[*]

(LHCb Collaboration)

The properties of the orbitally excited ($L = 1$) B_s^0 states are studied by using 1.0 fb^{-1} of pp collisions at $\sqrt{s} = 7$ TeV collected with the LHCb detector. The first observation of the $B_{s2}^*(5840)^0$ meson decaying to $B^{*+}K^-$ is reported, and the corresponding branching fraction measured relative to the B^+K^- decay mode. The $B_{s1}(5830)^0 \to B^{*+}K^-$ decay is observed as well. The width of the $B_{s2}^*(5840)^0$ state is measured for the first time, and the masses of the two states are determined with the highest precision to date. The observation of the $B_{s2}^*(5840)^0 \to B^{*+}K^-$ decay favors the spin-parity assignment $J^P = 2^+$ for the $B_{s2}^*(5840)^0$ meson. In addition, the most precise measurement of the mass difference $m(B^{*+}) - m(B^+) = 45.01 \pm 0.30(\text{stat}) \pm 0.23(\text{syst})$ MeV/c^2 is obtained.

Heavy quark effective theory describes mesons with one heavy and one light quark where the heavy quark is assumed to have infinite mass [1]. It is an important tool for calculating meson properties which may be modified by physics beyond the standard model, such as CP violation in charm meson decays [2] or the mixing and lifetimes of B mesons [3]. It also predicts the properties of excited B and B_s^0 mesons [4–7], and precise measurements of these properties are a sensitive test of the validity of the theory. Within heavy quark effective theory the B_s^0 mesons are characterized by three quantum numbers: the relative orbital angular momentum L of the two quarks, the total angular momentum of the light quark $j_q = |L \pm \frac{1}{2}|$, and the total angular momentum of the B_s^0 meson $J = |j_q \pm \frac{1}{2}|$. For $L = 1$ there are four different possible (J, j_q) combinations, all with even parity. These are collectively termed the orbitally excited states. Such states can decay to B^+K^- and/or $B^{*+}K^-$ (the inclusion of charge-conjugate states is implied throughout this Letter), depending on their quantum numbers and mass values. The two states with $j_q = 1/2$, named B_{s0}^* and B'_{s1}, are expected to decay through an S-wave transition and to have a large $O(100$ MeV/$c^2)$ decay width. In contrast, the two states with $j_q = 3/2$, named $B_{s1}(5830)^0$ and $B_{s2}^*(5840)^0$ (henceforth B_{s1} and B_{s2}^* for brevity), are expected to decay through a D-wave transition and to have a narrow $O(1$ MeV/$c^2)$ decay width. Table I gives an overview of these states.

In this Letter, a 1.0 fb^{-1} sample of data collected by the LHCb detector is used to search for the orbitally excited B_s^0 mesons in the mass distribution of B^+K^- pairs, where the B^+ mesons are selected in the four decay modes:

$B^+ \to J/\psi(\mu^+\mu^-)K^+$, $B^+ \to \bar{D}^0(K^+\pi^-)\pi^+$, $B^+ \to \bar{D}^0(K^+\pi^-\pi^+\pi^-)\pi^+$, and $B^+ \to \bar{D}^0(K^+\pi^-)\pi^+\pi^-\pi^+$. Two narrow peaks were observed in the B^+K^- mass distribution by the CDF Collaboration [9]. Putatively, they are identified with the states of the $j_q = 3/2$ doublet expected in heavy quark effective theory [4] and are named B_{s1} and B_{s2}^*. As the $B_{s1} \to B^+K^-$ decay is forbidden, one of the mass peaks observed is interpreted as the $B_{s1} \to B^{*+}K^-$ decay followed by $B^{*+} \to B^+\gamma$, where the photon is not observed. This peak is shifted by the $B^{*+} - B^+$ mass difference due to the missing momentum of the photon in the $B^{*+} \to B^+\gamma$ decay. While the $B_{s2}^* \to B^+K^-$ decay has been observed by the D0 Collaboration as well [10], a confirmation of the B_{s1} meson is still missing. The identification of the B_{s1} and B_{s2}^* mesons in the B^+K^- mass spectrum is based on the expected mass splitting between the $j_q = 3/2$ states. The B_{s1} and B_{s2}^* widths are very sensitive to their masses, due to their proximity to the BK and B^*K thresholds. Measurements of the widths thus provide fundamental information concerning the nature of these states. In addition, the B_{s1} and B_{s2}^* quantum numbers have not yet been directly determined, and the observation of other decay modes can constrain the spin-parity combinations of the states. In particular, the $B_{s2}^* \to B^{*+}K^-$ decay has not yet been observed but could manifest itself in the B^+K^- mass spectrum in a similar fashion to the corresponding B_{s1} meson decay. The $B_{s2}^* \to B^{*+}K^-$ branching fraction relative to $B_{s2}^* \to B^+K^-$ is predicted to

*Full author list given at the end of the article.

TABLE I. Summary of the orbitally excited ($L = 1$) B_s^0 states.

| | j_q | J^P | Allowed decay mode | | Mass (MeV/c^2) [8] |
			B^+K^-	$B^{*+}K^-$	
B_{s0}^*	1/2	0^+	Yes	No	Unobserved
B'_{s1}	1/2	1^+	No	Yes	Unobserved
B_{s1}	3/2	1^+	No	Yes	5829.4 ± 0.7
B_{s2}^*	3/2	2^+	Yes	Yes	5839.7 ± 0.6

be between 2% and 10%, depending on the B_{s2}^* mass [11–14].

Recently, the Belle Collaboration has reported observation of charged bottomoniumlike $Z_b(10610)^+$ and $Z_b(10650)^+$ states [15,16] that could be interpreted as $B\bar{B}^*$ and $B^*\bar{B}^*$ molecules, respectively [17]. To test this interpretation, improved measurements of the B^{*+} mass are necessary and can be obtained from the difference in peak positions between $B_{s2}^* \to B^{*+}K^-$ and $B_{s2}^* \to B^+K^-$ decays in the B^+K^- mass spectrum.

The LHCb detector [18] is a single-arm forward spectrometer covering the pseudorapidity range $2 < \eta < 5$, designed for studying particles containing b or c quarks. The detector includes a high-precision tracking system consisting of a silicon-strip vertex detector surrounding the pp interaction region, a large-area silicon-strip detector located upstream of a dipole magnet with a bending power of about 4 Tm, and three stations of silicon-strip detectors and straw drift tubes placed downstream. The combined tracking system has a momentum resolution $(\Delta p/p)$, that varies from 0.4% at 5 GeV/c to 0.6% at 100 GeV/c, and a decay time resolution of 50 fs. The resolution of the impact parameter, the transverse distance of closest approach between the track and a primary interaction, is about 20 μm for tracks with large transverse momentum. The transverse component is measured in the plane normal to the beam axis. Charged hadrons are identified by using two ring-imaging Cherenkov detectors. Photon, electron, and hadron candidates are identified by a calorimeter system consisting of scintillating-pad and preshower detectors, an electromagnetic calorimeter, and a hadronic calorimeter. Muons are identified by a system composed of alternating layers of iron and multiwire proportional chambers.

The trigger system [19] consists of a hardware stage, based on information from the calorimeter and muon systems, followed by a software stage that applies a full event reconstruction. Events likely to contain a B meson are selected by searching for a dimuon vertex detached from the primary interaction or two-, three-, and four-track vertices detached from the primary interaction which have high total transverse momentum. These are, respectively, referred to as dimuon and topological triggers.

The samples of simulated events used in this analysis are based on the PYTHIA 6.4 generator [20], with a choice of parameters specifically configured for LHCb [21]. The EVTGEN package [22] describes the decay of the B mesons, and the GEANT4 toolkit [23,24] is used to simulate the detector response. QED radiative corrections are generated with the PHOTOS package [25].

In the offline analysis the B mesons are reconstructed by using a set of loose selection criteria to suppress the majority of the combinatorial backgrounds. The $B^+ \to J/\psi K^+$ selection requires a B^+ candidate with a transverse momentum of at least 2 GeV/c and a decay time of at least 0.3 ps. For the other decay modes, the selection explicitly

requires that the topological trigger, which selected the event, is based exclusively on tracks from which the B meson candidate is formed. Additional loose selection requirements are placed on variables related to the B meson production and decay such as transverse momentum and quality of the track fits for the decay products, detachment of the B^+ candidate from the primary interaction, whether the momentum of the B^+ candidate points back to the primary interaction, and the impact parameter χ^2. The impact parameter χ^2 is defined as the difference between the χ^2 of the primary vertex reconstructed with and without the considered track.

Following these selections, B^+ signals are visible above backgrounds in all four decay modes. In order to improve their purity, four boosted decision tree classifiers [26] are trained on variables common to all four decay modes: the transverse momenta and impact parameters of the final state tracks, the transverse momentum and impact parameter of the B^+ candidate, the detachment of the B^+ candidate from the primary interaction, the cosine of the angle between the B^+ candidate momentum and the direction of flight from the primary vertex to the decay vertex, the fit χ^2 of the tracks, and particle identification information. The classifier is trained on data by using the *sWeights* technique [27], with the B^+ candidate mass as a discriminating variable, to unfold the signal and background distributions. The cut on the classifier response is chosen by optimizing the significance of each B^+ signal. The final mass distributions for the B^+ candidates are shown in Fig. 1.

The B^+ candidate mass spectra are fitted by using a double Gaussian function for the signal and a second-order polynomial for the background. The average mass resolution σ_{B^+} is defined as the weighted average of the Gaussian widths. The purities of the samples, defined as the fraction of the signal events in a $\pm 2\sigma_{B^+}$ mass region, are 96%, 91%, 90%, and 85% for the $B^+ \to J/\psi K^+$, $B^+ \to \bar{D}^0(K^+\pi^-)\pi^+$, $B^+ \to \bar{D}^0(K^+\pi^-\pi^+\pi^-)\pi^+$, and $B^+ \to \bar{D}^0(K^+\pi^-)\pi^+\pi^-\pi^+$ decays, respectively. The B^+ candidates, within a $\pm 2\sigma_{B^+}$ mass region, are selected for each decay mode. A sample of about 1 000 000 B^+ candidates is obtained and combined with any track of opposite charge that is identified as a kaon.

Multiple pp interactions can occur in LHC bunch crossings. In order to reduce combinatorial backgrounds, the B^+ and kaon candidates are required to be consistent with coming from the same interaction point. The signal purity is improved by a boosted decision tree classifier, whose inputs are the B^+ and the kaon transverse momenta, the log-likelihood difference between the kaon and pion hypotheses, and the vertex fit and impact parameter χ^2. The training is performed by using simulated events for the signal and the like-charge B^+K^+ candidates in the data for the background. The same selection is subsequently applied to all B^+ decay modes. The cut on the classifier response is chosen by optimizing the significance of the
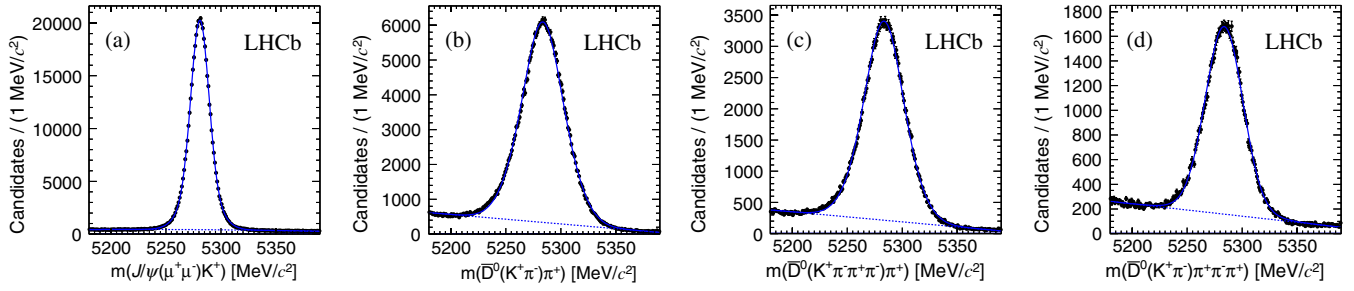
FIG. 1 (color online).   Invariant mass spectra of the final B^+ candidates. The signal line shape is fitted with a double Gaussian distribution, while the background is modeled with a second-order polynomial. (a) $B^+ \to J/\psi K^+$, (b) $B^+ \to \bar{D}^0(K^+\pi^-)\pi^+$, (c) $B^+ \to \bar{D}^0(K^+\pi^-\pi^+\pi^-)\pi^+$, and (d) $B^+ \to \bar{D}^0(K^+\pi^-)\pi^+\pi^-\pi^+$ decays. The J/ψ and D^0 masses are constrained to their world average values.

$B_{s2}^* \to B^+K^-$ signal. It retains 57% of the signal events and rejects 92% of the background events. In order to improve the mass resolution, the B^+K^- mass fits are performed by constraining the J/ψ (or D^0) and B^+ particles to their respective world average masses [8] and constraining the B^+ and K^- momenta to point to the associated primary vertex.

Figure 2 shows the mass difference for the selected candidates, summed over all B^+ decay modes. The mass difference is defined as $Q \equiv m(B^+K^-) - m(B^+) - m(K^-)$, where $m(B^+)$ and $m(K^-)$ are the known masses of the B^+ and K^- mesons [8], respectively. The two narrow peaks at 10 and 67 MeV/c^2 are identified as the $B_{s1} \to B^{*+}K^-$ and $B_{s2}^* \to B^+K^-$ signals, respectively, as previously observed. In addition, a smaller structure is seen around 20 MeV/c^2, identified as the previously unobserved $B_{s2}^* \to B^{*+}K^-$ decay mode.

Simulated events are used to compute the detector resolutions corresponding to the three signals. The values obtained are increased by 20% to account for differences
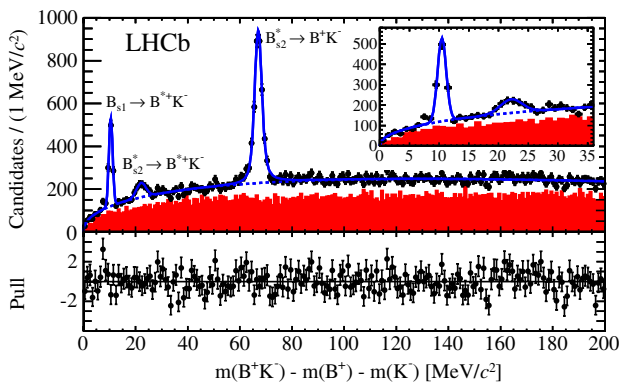

FIG. 2 (color online). Mass difference distribution $m(B^+K^-) - m(B^+) - m(K^-)$. The three peaks are identified as (left) $B_{s1} \to B^{*+}K^-$, (middle) $B_{s2}^* \to B^{*+}K^-$, and (right) $B_{s2}^* \to B^+K^-$. The total fit function is shown as a solid blue line, while the shaded red region is the spectrum of like-charge B^+K^+ combinations. The inset shows an expanded view of the $B_{s1}/B_{s2}^* \to B^{*+}K^-$ signals. The bottom plot shows the fit pulls.

between the B^+ resolutions in data and simulated events. The corrected resolutions are 0.4, 0.6, and 1.0 MeV/c^2 for the $B_{s1} \to B^{*+}K^-$, $B_{s2}^* \to B^{*+}K^-$, and $B_{s2}^* \to B^+K^-$ signals, respectively. A discrepancy of 40% between the mass resolutions in data and simulated events is observed for decays with small Q values, such as $D^{*+} \to D^0\pi^+$. Therefore we assign an uncertainty of $\pm 20\%$ to the resolution in the systematic studies.

An unbinned fit of the mass difference distribution is performed to extract the Q values and event yields of the three peaks. The $B_{s2}^* \to B^+K^-$ signal is parameterized by a relativistic Breit-Wigner function with natural width Γ convolved with a Gaussian function that accounts for the detector resolution. Its width is fixed to the value obtained from simulated events. The line shapes of the $B_{s1}/B_{s2}^* \to B^{*+}K^-$ signals, expected to be Breit-Wigner functions in the $B^{*+}K^-$ mass spectrum, are affected by the phase space and the angular distribution of the decays, as the photon is not reconstructed. The resulting shapes cannot be properly simulated due to the lack of knowledge of the B_{s1}/B_{s2}^* properties. Therefore, a Gaussian function is used for each $B_{s1}/B_{s2}^* \to B^{*+}K^-$ signal as effective parameterization. The background is modeled by a threshold function $f(Q) = Q^\alpha e^{\beta Q + \delta}$, where α, β, and δ are free parameters in the fit. Its analytical form is verified by fitting the like-charge B^+K^+ combinations where no signal is expected.

The parameters allowed to vary in the fit are the yield $N_{B_{s2}^* \to B^+K^-}$, the yield ratios $N_{B_{s1} \to B^{*+}K^-}/N_{B_{s2}^* \to B^+K^-}$ and $N_{B_{s2}^* \to B^{*+}K^-}/N_{B_{s2}^* \to B^+K^-}$, the Q values of the $B_{s1} \to B^{*+}K^-$ and $B_{s2}^* \to B^+K^-$ signals, the mass difference between the $B_{s2}^* \to B^+K^-$ and $B_{s2}^* \to B^{*+}K^-$ peaks, the natural width of the B_{s2}^* state, the Gaussian widths of $B_{s1}/B_{s2}^* \to B^{*+}K^-$ signals, and the parameters of the threshold function. From the yield ratios, the relative branching fraction

$$\frac{\mathcal{B}(B_{s2}^* \to B^{*+}K^-)}{\mathcal{B}(B_{s2}^* \to B^+K^-)} = \frac{N_{B_{s2}^* \to B^{*+}K^-}}{N_{B_{s2}^* \to B^+K^-}} \times \epsilon_{2,2}^{\text{rel}} = R^{B_{s2}^*} \quad (1)$$

TABLE II.   Results of the fit to the mass difference distributions $m(B^+K^-) - m(B^+) - m(K^-)$. The first uncertainties are statistical, and the second are systematic.

Parameter	Fit result	Best previous measurement
$m(B_{s1}) - m(B^{*+}) - m(K^-)$	$10.46 \pm 0.04 \pm 0.04$ MeV/c^2	$10.73 \pm 0.21 \pm 0.14$ MeV/c^2 [9]
$m(B_{s2}^*) - m(B^+) - m(K^-)$	$67.06 \pm 0.05 \pm 0.11$ MeV/c^2	$66.96 \pm 0.39 \pm 0.14$ MeV/c^2 [9]
$m(B^{*+}) - m(B^+)$	$45.01 \pm 0.30 \pm 0.23$ MeV/c^2	45.6 ± 0.8 MeV/c^2 [28]
$\Gamma(B_{s2}^*)$	$1.56 \pm 0.13 \pm 0.47$ MeV/c^2	
$\frac{\mathcal{B}(B_{s2}^* \to B^{*+}K^-)}{\mathcal{B}(B_{s2}^* \to B^+K^-)}$	$(9.3 \pm 1.3 \pm 1.2)\%$	
$\frac{\sigma(pp \to B_{s1}X)\mathcal{B}(B_{s1} \to B^{*+}K^-)}{\sigma(pp \to B_{s2}^*X)\mathcal{B}(B_{s2}^* \to B^+K^-)}$	$(23.2 \pm 1.4 \pm 1.3)\%$	
$N_{B_{s1} \to B^{*+}K^-}$	750 ± 36	
$N_{B_{s2}^* \to B^{*+}K^-}$	307 ± 46	
$N_{B_{s2}^* \to B^+K^-}$	3140 ± 100	

is measured. The B_{s1} to B_{s2}^* ratio of production cross sections times the ratio of branching fractions of $B_{s1} \to B^{*+}K^-$ relative to that of $B_{s2}^* \to B^+K^-$ is also determined from

$$\frac{\sigma(pp \to B_{s1}X)\mathcal{B}(B_{s1} \to B^{*+}K^-)}{\sigma(pp \to B_{s2}^*X)\mathcal{B}(B_{s2}^* \to B^+K^-)}$$
$$= \frac{N_{B_{s1} \to B^{*+}K^-}}{N_{B_{s2}^* \to B^+K^-}} \times \epsilon_{1,2}^{\text{rel}} = \sigma^{B_{s1}/B_{s2}^*} R^{B_{s1}/B_{s2}^*}. \quad (2)$$

These ratios are corrected by the relative selection efficiencies $\epsilon_{2,2}^{\text{rel}} = 1.05 \pm 0.02$ and $\epsilon_{1,2}^{\text{rel}} = 1.03 \pm 0.01$, using simulated decays. The fit results are given in Table II. The widths of the two Gaussian functions are 0.73 ± 0.04 and 1.9 ± 0.3 MeV/c^2 for the $B_{s1} \to B^{*+}K^-$ and $B_{s2}^* \to B^{*+}K^-$ signals, respectively. A binned χ^2 test gives a confidence level of 43% for the fit.

To determine the significance of the $B_{s2}^* \to B^{*+}K^-$ signal, a similar maximum likelihood fit is performed, where all parameters of the signal are fixed according to expectation, except its yield. The likelihood of this fit is compared to the result of a fit where the yield of the signal is fixed to zero. The statistical significance of the $B_{s2}^* \to B^{*+}K^-$ signal is 8σ.

A number of systematic uncertainties are considered. For the signal model, the signal shape is changed to a double Gaussian function and an alternative threshold function is used for the background. The changes in the fit results are assigned as the associated uncertainties. The B^+ decay modes are fitted independently to test for effects that may be related to differences in their selection requirements. For each observable quoted in Table II, the difference between the weighted average of these independent fits and the global fit is taken as a systematic uncertainty. Additional systematic uncertainties are assigned based on the change in the results when varying the selection criteria and the B^+ signal region. The detector resolution of $B_{s2}^* \to B^+K^-$ signal is varied by $\pm 20\%$. In addition, the momentum scale in the processing of the data used in this analysis is varied within the estimated uncertainty of 0.15%. The corresponding uncertainty on the measured masses is assigned as a systematic uncertainty. The uncertainty on the determination of the selection efficiency ratios caused by finite samples of simulated events is taken as a systematic uncertainty for the branching fractions. Finally, simulated events are used to estimate the mass shifts of the $B_{s1}/B_{s2}^* \to B^{*+}K^-$ signals from the nominal values when the radiated photon is excluded from their reconstructed decays. The absolute systematic uncertainties are given in Table III. The $B_{s2}^* \to B^{*+}K^-$ signal is observed with the expected frequency in each of the four resconstructed

TABLE III.   Absolute systematic uncertainties for each measurement, which are assumed to be independent and are added in quadrature.

Source	$Q(B_{s1})$ (MeV/c^2)	$Q(B_{s2}^*)$ (MeV/c^2)	$m(B^{*+}) - m(B^+)$ (MeV/c^2)	$\Gamma(B_{s2}^*)$ (MeV/c^2)	$R^{B_{s2}^*}$ (%)	$\sigma^{B_{s1}/B_{s2}^*}R^{B_{s1}/B_{s2}^*}$ (%)
Fit model	0.00	0.02	0.03	0.01	0.2	0.5
B^+ decay mode	0.01	0.01	0.02	0.01	0.1	0.1
Selection	0.03	0.02	0.19	0.05	1.1	0.6
B^+ signal region	0.01	0.03	0.11	0.07	0.2	0.4
Mass resolution	0.00	0.01	0.02	0.46	0.2	0.9
Momentum scale	0.02	0.10	0.03	$\cdots$	$\cdots$	$\cdots$
Efficiency ratios	$\cdots$	$\cdots$	$\cdots$	$\cdots$	0.2	0.2
Missing photon	0.01	$\cdots$	0.01	$\cdots$	$\cdots$	$\cdots$
Total	0.04	0.11	0.23	0.47	1.2	1.3

decay modes, and the systematic error for the $\frac{\mathcal{B}(B_{s2}^* \to B^{*+}K^-)}{\mathcal{B}(B_{s2}^* \to B^+K^-)}$ branching fraction ratio, related to the different B^+ decay modes, is small. The final results are shown in Table II. The measured mass differences are more precise than the previous best measurements of a factor of 2 at least. The measured $\frac{\mathcal{B}(B_{s2}^* \to B^{*+}K^-)}{\mathcal{B}(B_{s2}^* \to B^+K^-)}$ branching fraction ratio and B_{s2}^* width are in good agreement with theoretical predictions [12–14].

The mass differences given in Table II are translated into absolute masses by adding the masses of the B^+ and kaon [8] and, in the case of the B_{s1} meson, the $B^{*+} - B^+$ mass difference measured in this Letter. The results are

$$m(B^{*+}) = 5324.26 \pm 0.30 \pm 0.23 \pm 0.17 \text{ MeV}/c^2,$$

$$m(B_{s1}) = 5828.40 \pm 0.04 \pm 0.04 \pm 0.41 \text{ MeV}/c^2,$$

$$m(B_{s2}^*) = 5839.99 \pm 0.05 \pm 0.11 \pm 0.17 \text{ MeV}/c^2,$$

where the first uncertainty is statistical and the second is systematic. The third uncertainty corresponds to the uncertainty on the B^+ mass [8] and, in the case of the B_{s1} mass measurement, the uncertainty on the $B^{*+} - B^+$ mass difference measured in this analysis.

The significance of the nonzero B_{s2}^* width is determined by comparing the likelihood for the nominal fit with a fit in which the width is fixed to zero. To account for systematic effects, the minimum $\sqrt{2\Delta \log \mathcal{L}}$ among all systematic variations is taken; the significance including systematic uncertainties is 9σ.

In conclusion, by using 1.0 fb^{-1} of data collected with the LHCb detector at $\sqrt{s} = 7$ TeV, the decay mode $B_{s2}^* \to B^{*+}K^-$ is observed for the first time and its branching fraction measured relative to that of $B_{s2}^* \to B^+K^-$. The observation of the B_{s2}^* meson decaying to two pseudoscalars ($B_{s2}^* \to B^+K^-$) and to a vector and a pseudoscalar ($B_{s2}^* \to B^{*+}K^-$) favors the assignment of $J^P = 2^+$ for this state. The B_{s2}^* width is measured for the first time, while the masses of the B_{s1} and B_{s2}^* states are measured with the highest precision to date and are consistent with previous measurements [9,10]. Finally, the observed $B_{s2}^* \to B^{*+}K^-$ decay is used to make the most precise measurement to date of the $B^{*+} - B^+$ mass difference. This measurement, unlike others reported in the literature, does not require the reconstruction of the soft photon from B^{*+} decays and therefore has significantly smaller systematic uncertainty. High precision measurements of the B^{*+} mass are important for the understanding of the exotic Z_b^+ states recently observed [15]. Using the B^{*+} mass measured in this analysis, we compute that the $Z_b(10610)^+$ and $Z_b(10650)^+$ masses are 3.69 ± 2.05 and 3.68 ± 1.71 MeV/c^2 above the $B\bar{B}^*$ and $B^*\bar{B}^*$ thresholds, respectively.

[1] T. Mannel, arXiv:hep-ph/9611411.
[2] M. Bobrowski, A. Lenz, J. Riedl, and J. Rohrwild, J. High Energy Phys. 03 (2010) 009.
[3] A. Lenz, arXiv:1205.1444.
[4] M. Di Pierro and E. Eichten, Phys. Rev. D **64**, 114004 (2001).
[5] E. J. Eichten, C. T. Hill, and C. Quigg, Phys. Rev. Lett. **71**, 4116 (1993).
[6] A. F. Falk and T. Mehen, Phys. Rev. D **53**, 231 (1996).
[7] J. Koponen (UKQCD Collaboration), Phys. Rev. D **78**, 074509 (2008).
[8] J. Beringer et al. (Particle Data Group), Phys. Rev. D **86**, 010001 (2012).
[9] T. Aaltonen et al. (CDF Collaboration), Phys. Rev. Lett. **100**, 082001 (2008).
[10] V. Abazov et al. (D0 Collaboration), Phys. Rev. Lett. **100**, 082002 (2008).
[11] S. Godfrey and R. Kokoski, Phys. Rev. D **43**, 1679 (1991).
[12] P. Colangelo, F. De Fazio, F. Giannuzzi, and S. Nicotri, Phys. Rev. D **86**, 054024 (2012).
[13] X.-H. Zhong and Q. Zhao, Phys. Rev. D **78**, 014029 (2008).
[14] Z.-H. Wang, G.-L. Wang, H.-F. Fu, and Y. Jiang, Phys. Lett. B **706**, 389 (2012).
[15] A. Bondar et al. (Belle Collaboration), Phys. Rev. Lett. **108**, 122001 (2012).
[16] I. Adachi et al. (Belle Collaboration), arXiv:1209.6450.
[17] A. Bondar, A. Garmash, A. I. Milstein, R. Mizuk, and M. B. Voloshin, Phys. Rev. D **84**, 054010 (2011).
[18] A. A. Alves, Jr. et al. (LHCb Collaboration), JINST **3**, S08005 (2008).
[19] R. Aaij et al., arXiv:1211.3055.
[20] T. Sjöstrand, S. Mrenna, and P. Skands, J. High Energy Phys. 05 (2006) 026.
[21] I. Belyaev et al., in Proceedings of the 2010 IEEE Nuclear Science Symposium Conference (IEEE, New York, 2010), p. 1155.

[22] D. J. Lange, Nucl. Instrum. Methods Phys. Res., Sect. A **462**, 152 (2001).

[23] J. Allison *et al.* (GEANT4 Collaboration), IEEE Trans. Nucl. Sci. **53**, 270 (2006); S. Agostinelli *et al.* (GEANT4 Collaboration), Nucl. Instrum. Methods Phys. Res., Sect. A **506**, 250 (2003).

[24] M. Clemencic, G. Corti, S. Easo, C. R. Jones, S. Miglioranzi, M. Pappagallo, and P. Robbe, J. Phys. Conf. Ser. **331**, 032023 (2011).

[25] P. Golonka and Z. Was, Eur. Phys. J. C **45**, 97 (2006).

[26] L. Breiman, J. H. Friedman, R. A. Olshen, and C. J. Stone, *Classification and Regression Trees* (Wadsworth International Group, Belmont, CA, 1984); B. P. Roe, H.-J. Yang, J. Zhu, Y. Liu, I. Stancu, and G. McGregor, Nucl. Instrum. Methods Phys. Res., Sect. A **543**, 577 (2005).

[27] M. Pivk and F. R. Le Diberder, Nucl. Instrum. Methods Phys. Res., Sect. A **555**, 356 (2005).

[28] Q. Wu, P. Franzini, S. Kanekal, P. M. Tuts, U. Heintz, J. Lee-Franzini, M. Narain, R. D. Schamberger, J. Willins, and C. Yanagisawa, Phys. Lett. B **273**, 177 (1991).

R. Aaij,[38] C. Abellan Beteta,[33,n] A. Adametz,[11] B. Adeva,[34] M. Adinolfi,[43] C. Adrover,[6] A. Affolder,[49] Z. Ajaltouni,[5] J. Albrecht,[35] F. Alessio,[35] M. Alexander,[48] S. Ali,[38] G. Alkhazov,[27] P. Alvarez Cartelle,[34] A. A. Alves, Jr.,[22] S. Amato,[2] Y. Amhis,[36] L. Anderlini,[17,f] J. Anderson,[37] R. B. Appleby,[51] O. Aquines Gutierrez,[10] F. Archilli,[18,35] A. Artamonov,[32] M. Artuso,[53] E. Aslanides,[6] G. Auriemma,[22,m] S. Bachmann,[11] J. J. Back,[45] C. Baesso,[54] W. Baldini,[16] R. J. Barlow,[51] C. Barschel,[35] S. Barsuk,[7] W. Barter,[44] A. Bates,[48] Th. Bauer,[38] A. Bay,[36] J. Beddow,[48] I. Bediaga,[1] S. Belogurov,[28] K. Belous,[32] I. Belyaev,[28] E. Ben-Haim,[8] M. Benayoun,[8] G. Bencivenni,[18] S. Benson,[47] J. Benton,[43] A. Berezhnoy,[29] R. Bernet,[37] M.-O. Bettler,[44] M. van Beuzekom,[38] A. Bien,[11] S. Bifani,[12] T. Bird,[51] A. Bizzeti,[17,h] P. M. Bjørnstad,[51] T. Blake,[35] F. Blanc,[36] C. Blanks,[50] J. Blouw,[11] S. Blusk,[53] A. Bobrov,[31] V. Bocci,[22] A. Bondar,[31] N. Bondar,[27] W. Bonivento,[15] S. Borghi,[51] A. Borgia,[53] T. J. V. Bowcock,[49] C. Bozzi,[16] T. Brambach,[9] J. van den Brand,[39] J. Bressieux,[36] D. Brett,[51] M. Britsch,[10] T. Britton,[53] N. H. Brook,[43] H. Brown,[49] A. Büchler-Germann,[37] I. Burducea,[26] A. Bursche,[37] J. Buytaert,[35] S. Cadeddu,[15] O. Callot,[7] M. Calvi,[20,j] M. Calvo Gomez,[33,n] A. Camboni,[33] P. Campana,[18,35] A. Carbone,[14,c] G. Carboni,[21,k] R. Cardinale,[19,i] A. Cardini,[15] H. Carranza-Mejia,[47] L. Carson,[50] K. Carvalho Akiba,[2] G. Casse,[49] M. Cattaneo,[35] Ch. Cauet,[9] M. Charles,[52] Ph. Charpentier,[35] P. Chen,[3,36] N. Chiapolini,[37] M. Chrzaszcz,[23] K. Ciba,[35] X. Cid Vidal,[34] G. Ciezarek,[50] P. E. L. Clarke,[47] M. Clemencic,[35] H. V. Cliff,[44] J. Closier,[35] C. Coca,[26] V. Coco,[38] J. Cogan,[6] E. Cogneras,[5] P. Collins,[35] A. Comerma-Montells,[33] A. Contu,[15] A. Cook,[43] M. Coombes,[43] G. Corti,[35] B. Couturier,[35] G. A. Cowan,[36] D. C. Craik,[45] S. Cunliffe,[50] R. Currie,[47] C. D'Ambrosio,[35] P. David,[8] P. N. Y. David,[38] I. De Bonis,[4] K. De Bruyn,[38] S. De Capua,[51] M. De Cian,[37] J. M. De Miranda,[1] L. De Paula,[2] P. De Simone,[18] D. Decamp,[4] M. Deckenhoff,[9] H. Degaudenzi,[36,35] L. Del Buono,[8] C. Deplano,[15] D. Derkach,[14] O. Deschamps,[5] F. Dettori,[39] A. Di Canto,[11] J. Dickens,[44] H. Dijkstra,[35] P. Diniz Batista,[1] M. Dogaru,[26] F. Domingo Bonal,[33,n] S. Donleavy,[49] F. Dordei,[11] A. Dosil Suárez,[34] D. Dossett,[45] A. Dovbnya,[40] F. Dupertuis,[36] R. Dzhelyadin,[32] A. Dziurda,[23] A. Dzyuba,[27] S. Easo,[46,35] U. Egede,[50] V. Egorychev,[28] S. Eidelman,[31] D. van Eijk,[38] S. Eisenhardt,[47] U. Eitschberger,[9] R. Ekelhof,[9] L. Eklund,[48,35] I. El Rifai,[5] Ch. Elsasser,[37] D. Elsby,[42] A. Falabella,[14,e] C. Färber,[11] G. Fardell,[47] C. Farinelli,[38] S. Farry,[12] V. Fave,[36] D. Ferguson,[47] V. Fernandez Albor,[34] F. Ferreira Rodrigues,[1] M. Ferro-Luzzi,[35] S. Filippov,[30] M. Fiore,[16] C. Fitzpatrick,[35] M. Fontana,[10] F. Fontanelli,[19,i] R. Forty,[35] O. Francisco,[2] M. Frank,[35] C. Frei,[35] M. Frosini,[17,f] S. Furcas,[20] A. Gallas Torreira,[34] D. Galli,[14,c] M. Gandelman,[2] P. Gandini,[52] Y. Gao,[3] J-C. Garnier,[35] J. Garofoli,[53] P. Garosi,[51] J. Garra Tico,[44] L. Garrido,[33] C. Gaspar,[35] R. Gauld,[52] E. Gersabeck,[11] M. Gersabeck,[35] T. Gershon,[45,35] Ph. Ghez,[4] V. Gibson,[44] V. V. Gligorov,[35] C. Göbel,[54] D. Golubkov,[28] A. Golutvin,[50,28,35] A. Gomes,[2] H. Gordon,[52] M. Grabalosa Gándara,[33] R. Graciani Diaz,[33] L. A. Granado Cardoso,[35] E. Graugés,[33] G. Graziani,[17] A. Grecu,[26] E. Greening,[52] S. Gregson,[44] O. Grünberg,[55] B. Gui,[53] E. Gushchin,[30] Yu. Guz,[32,35] T. Gys,[35] C. Hadjivasiliou,[53] G. Haefeli,[36] C. Haen,[35] S. C. Haines,[44] S. Hall,[50] T. Hampson,[43] S. Hansmann-Menzemer,[11] N. Harnew,[52] S. T. Harnew,[43] J. Harrison,[51] P. F. Harrison,[45] T. Hartmann,[55] J. He,[7] V. Heijne,[38] K. Hennessy,[49] P. Henrard,[5] J. A. Hernando Morata,[34] E. van Herwijnen,[35] E. Hicks,[49] D. Hill,[52] M. Hoballah,[5] P. Hopchev,[4] W. Hulsbergen,[38] P. Hunt,[52] T. Huse,[49] N. Hussain,[52] D. Hutchcroft,[49] D. Hynds,[48] V. Iakovenko,[41] P. Ilten,[12] J. Imong,[43] R. Jacobsson,[35] A. Jaeger,[11] M. Jahjah Hussein,[5] E. Jans,[38] F. Jansen,[38] P. Jaton,[36] B. Jean-Marie,[7] F. Jing,[3] M. John,[52] D. Johnson,[52] C. R. Jones,[44] B. Jost,[35] M. Kaballo,[9] S. Kandybei,[40] M. Karacson,[35] T. M. Karbach,[35] I. R. Kenyon,[42] U. Kerzel,[35] T. Ketel,[39] A. Keune,[36] B. Khanji,[20] Y. M. Kim,[47] O. Kochebina,[7] V. Komarov,[36] R. F. Koopman,[39] P. Koppenburg,[38] M. Korolev,[29] A. Kozlinskiy,[38] L. Kravchuk,[30] K. Kreplin,[11] M. Kreps,[45] G. Krocker,[11] P. Krokovny,[31] F. Kruse,[9] M. Kucharczyk,[20,23,j] V. Kudryavtsev,[31] T. Kvaratskheliya,[28,35] V. N. La Thi,[36] D. Lacarrere,[35] G. Lafferty,[51] A. Lai,[15] D. Lambert,[47] R. W. Lambert,[39] E. Lanciotti,[35] G. Lanfranchi,[18,35] C. Langenbruch,[35] T. Latham,[45]

C. Lazzeroni,[42] R. Le Gac,[6] J. van Leerdam,[38] J.-P. Lees,[4] R. Lefèvre,[5] A. Leflat,[29] J. Lefrançois,[7] O. Leroy,[6]
T. Lesiak,[23] Y. Li,[3] L. Li Gioi,[5] M. Liles,[49] R. Lindner,[35] C. Linn,[11] B. Liu,[3] G. Liu,[35] J. von Loeben,[20] J. H. Lopes,[2]
E. Lopez Asamar,[33] N. Lopez-March,[36] H. Lu,[3] J. Luisier,[36] H. Luo,[47] A. Mac Raighne,[48] F. Machefert,[7]
I. V. Machikhiliyan,[4,28] F. Maciuc,[26] O. Maev,[27,35] J. Magnin,[1] M. Maino,[20] S. Malde,[52] G. Manca,[15,d]
G. Mancinelli,[6] N. Mangiafave,[44] U. Marconi,[14] R. Märki,[36] J. Marks,[11] G. Martellotti,[22] A. Martens,[8] L. Martin,[52]
A. Martín Sánchez,[7] M. Martinelli,[38] D. Martinez Santos,[39] D. Martins Tostes,[2] A. Massafferri,[1] R. Matev,[35]
Z. Mathe,[35] C. Matteuzzi,[20] M. Matveev,[27] E. Maurice,[6] A. Mazurov,[16,30,35,e] J. McCarthy,[42] G. McGregor,[51]
R. McNulty,[12] F. Meier,[9] M. Meissner,[11] M. Merk,[38] J. Merkel,[9] D. A. Milanes,[13] M.-N. Minard,[4]
J. Molina Rodriguez,[54] S. Monteil,[5] D. Moran,[51] P. Morawski,[23] R. Mountain,[53] I. Mous,[38] F. Muheim,[47] K. Müller,[37]
R. Muresan,[26] B. Muryn,[24] B. Muster,[36] J. Mylroie-Smith,[49] P. Naik,[43] T. Nakada,[36] R. Nandakumar,[46] I. Nasteva,[1]
M. Needham,[47] N. Neufeld,[35] A. D. Nguyen,[36] T. D. Nguyen,[36] C. Nguyen-Mau,[36,o] M. Nicol,[7] V. Niess,[5] R. Niet,[9]
N. Nikitin,[29] T. Nikodem,[11] A. Nomerotski,[52,35] A. Novoselov,[32] A. Oblakowska-Mucha,[24] V. Obraztsov,[32]
S. Oggero,[38] S. Ogilvy,[48] O. Okhrimenko,[41] R. Oldeman,[15,d] M. Orlandea,[26] J. M. Otalora Goicochea,[2] P. Owen,[50]
B. K. Pal,[53] A. Palano,[13,b] M. Palutan,[18] J. Panman,[35] A. Papanestis,[46] M. Pappagallo,[48] C. Parkes,[51]
C. J. Parkinson,[50] G. Passaleva,[17] G. D. Patel,[49] M. Patel,[50] G. N. Patrick,[46] C. Patrignani,[19,i] C. Pavel-Nicorescu,[26]
A. Pazos Alvarez,[34] A. Pellegrino,[38] G. Penso,[22,l] M. Pepe Altarelli,[35] S. Perazzini,[14,c] D. L. Perego,[20,j]
E. Perez Trigo,[34] A. Pérez-Calero Yzquierdo,[33] P. Perret,[5] M. Perrin-Terrin,[6] G. Pessina,[20] K. Petridis,[50]
A. Petrolini,[19,i] A. Phan,[53] E. Picatoste Olloqui,[33] B. Pie Valls,[33] B. Pietrzyk,[4] T. Pilař,[45] D. Pinci,[22] S. Playfer,[47]
M. Plo Casasus,[34] F. Polci,[8] G. Polok,[23] A. Poluektov,[45,31] E. Polycarpo,[2] D. Popov,[10] B. Popovici,[26] C. Potterat,[33]
A. Powell,[52] J. Prisciandaro,[36] V. Pugatch,[41] A. Puig Navarro,[36] W. Qian,[4] J. H. Rademacker,[43]
B. Rakotomiaramanana,[36] M. S. Rangel,[2] I. Raniuk,[40] N. Rauschmayr,[35] G. Raven,[39] S. Redford,[52] M. M. Reid,[45]
A. C. dos Reis,[1] S. Ricciardi,[46] A. Richards,[50] K. Rinnert,[49] V. Rives Molina,[33] D. A. Roa Romero,[5] P. Robbe,[7]
E. Rodrigues,[51] P. Rodriguez Perez,[34] G. J. Rogers,[44] S. Roiser,[35] V. Romanovsky,[32] A. Romero Vidal,[34]
J. Rouvinet,[36] T. Ruf,[35] H. Ruiz,[33] G. Sabatino,[22,k] J. J. Saborido Silva,[34] N. Sagidova,[27] P. Sail,[48] B. Saitta,[15,d]
C. Salzmann,[37] B. Sanmartin Sedes,[34] M. Sannino,[19,i] R. Santacesaria,[22] C. Santamarina Rios,[34] R. Santinelli,[35]
E. Santovetti,[21,k] M. Sapunov,[6] A. Sarti,[18,l] C. Satriano,[22,m] A. Satta,[21] M. Savrie,[16,e] D. Savrina,[28,29] P. Schaack,[50]
M. Schiller,[39] H. Schindler,[35] S. Schleich,[9] M. Schlupp,[9] M. Schmelling,[10] B. Schmidt,[35] O. Schneider,[36]
A. Schopper,[35] M.-H. Schune,[7] R. Schwemmer,[35] B. Sciascia,[18] A. Sciubba,[18,l] M. Seco,[34] A. Semennikov,[28]
K. Senderowska,[24] I. Sepp,[50] N. Serra,[37] J. Serrano,[6] P. Seyfert,[11] M. Shapkin,[32] I. Shapoval,[35,40] P. Shatalov,[28]
Y. Shcheglov,[27] T. Shears,[49,35] L. Shekhtman,[31] O. Shevchenko,[40] V. Shevchenko,[28] A. Shires,[50] R. Silva Coutinho,[45]
T. Skwarnicki,[53] N. A. Smith,[49] E. Smith,[52,46] M. Smith,[51] K. Sobczak,[5] F. J. P. Soler,[48] F. Soomro,[18] D. Souza,[43]
B. Souza De Paula,[2] B. Spaan,[9] A. Sparkes,[47] P. Spradlin,[48] F. Stagni,[35] S. Stahl,[11] O. Steinkamp,[37] S. Stoica,[26]
S. Stone,[53] B. Storaci,[38] M. Straticiuc,[26] U. Straumann,[37] V. K. Subbiah,[35] S. Swientek,[9] V. Syropoulos,[39]
M. Szczekowski,[25] P. Szczypka,[36,35] T. Szumlak,[24] S. T'Jampens,[4] M. Teklishyn,[7] E. Teodorescu,[26] F. Teubert,[35]
C. Thomas,[52] E. Thomas,[35] J. van Tilburg,[11] V. Tisserand,[4] M. Tobin,[37] S. Tolk,[39] D. Tonelli,[35] S. Topp-Joergensen,[52]
N. Torr,[52] E. Tournefier,[4,50] S. Tourneur,[36] M. T. Tran,[36] M. Tresch,[37] A. Tsaregorodtsev,[6] P. Tsopelas,[38] N. Tuning,[38]
M. Ubeda Garcia,[35] A. Ukleja,[25] D. Urner,[51] U. Uwer,[11] V. Vagnoni,[14] G. Valenti,[14] R. Vazquez Gomez,[33]
P. Vazquez Regueiro,[34] S. Vecchi,[16] J. J. Velthuis,[43] M. Veltri,[17,g] G. Veneziano,[36] M. Vesterinen,[35] B. Viaud,[7]
I. Videau,[7] D. Vieira,[2] X. Vilasis-Cardona,[33,n] J. Visniakov,[34] A. Vollhardt,[37] D. Volyanskyy,[10] D. Voong,[43]
A. Vorobyev,[27] V. Vorobyev,[31] C. Voß,[55] H. Voss,[10] R. Waldi,[55] R. Wallace,[12] S. Wandernoth,[11] J. Wang,[53]
D. R. Ward,[44] N. K. Watson,[42] A. D. Webber,[51] D. Websdale,[50] M. Whitehead,[45] J. Wicht,[35] D. Wiedner,[11]
L. Wiggers,[38] G. Wilkinson,[52] M. P. Williams,[45,46] M. Williams,[50,p] F. F. Wilson,[46] J. Wishahi,[9] M. Witek,[23]
W. Witzeling,[35] S. A. Wotton,[44] S. Wright,[44] S. Wu,[3] K. Wyllie,[35] Y. Xie,[47,35] F. Xing,[52] Z. Xing,[53] Z. Yang,[3]
R. Young,[47] X. Yuan,[3] O. Yushchenko,[32] M. Zangoli,[14] M. Zavertyaev,[10,a] F. Zhang,[3] L. Zhang,[53] W. C. Zhang,[12]
Y. Zhang,[3] A. Zhelezov,[11] A. Zhokhov,[28] L. Zhong,[3] and A. Zvyagin[35]

(LHCb Collaboration)

[1]*Centro Brasileiro de Pesquisas Físicas (CBPF), Rio de Janeiro, Brazil*
[2]*Universidade Federal do Rio de Janeiro (UFRJ), Rio de Janeiro, Brazil*
[3]*Center for High Energy Physics, Tsinghua University, Beijing, China*
[4]*LAPP, Université de Savoie, CNRS/IN2P3, Annecy-Le-Vieux, France*

[5]Clermont Université, Université Blaise Pascal, CNRS/IN2P3, LPC, Clermont-Ferrand, France
[6]CPPM, Aix-Marseille Université, CNRS/IN2P3, Marseille, France
[7]LAL, Université Paris-Sud, CNRS/IN2P3, Orsay, France
[8]LPNHE, Université Pierre et Marie Curie, Université Paris Diderot, CNRS/IN2P3, Paris, France
[9]Fakultät Physik, Technische Universität Dortmund, Dortmund, Germany
[10]Max-Planck-Institut für Kernphysik (MPIK), Heidelberg, Germany
[11]Physikalisches Institut, Ruprecht-Karls-Universität Heidelberg, Heidelberg, Germany
[12]School of Physics, University College Dublin, Dublin, Ireland
[13]Sezione INFN di Bari, Bari, Italy
[14]Sezione INFN di Bologna, Bologna, Italy
[15]Sezione INFN di Cagliari, Cagliari, Italy
[16]Sezione INFN di Ferrara, Ferrara, Italy
[17]Sezione INFN di Firenze, Firenze, Italy
[18]Laboratori Nazionali dell'INFN di Frascati, Frascati, Italy
[19]Sezione INFN di Genova, Genova, Italy
[20]Sezione INFN di Milano Bicocca, Milano, Italy
[21]Sezione INFN di Roma Tor Vergata, Roma, Italy
[22]Sezione INFN di Roma La Sapienza, Roma, Italy
[23]Henryk Niewodniczanski Institute of Nuclear Physics Polish Academy of Sciences, Kraków, Poland
[24]Faculty of Physics and Applied Computer Science, AGH-University of Science and Technology, Kraków, Poland
[25]National Center for Nuclear Research (NCBJ), Warsaw, Poland
[26]Horia Hulubei National Institute of Physics and Nuclear Engineering, Bucharest-Magurele, Romania
[27]Petersburg Nuclear Physics Institute (PNPI), Gatchina, Russia
[28]Institute of Theoretical and Experimental Physics (ITEP), Moscow, Russia
[29]Institute of Nuclear Physics, Moscow State University (SINP MSU), Moscow, Russia
[30]Institute for Nuclear Research of the Russian Academy of Sciences (INR RAN), Moscow, Russia
[31]Budker Institute of Nuclear Physics (SB RAS) and Novosibirsk State University, Novosibirsk, Russia
[32]Institute for High Energy Physics (IHEP), Protvino, Russia
[33]Universitat de Barcelona, Barcelona, Spain
[34]Universidad de Santiago de Compostela, Santiago de Compostela, Spain
[35]European Organization for Nuclear Research (CERN), Geneva, Switzerland
[36]Ecole Polytechnique Fédérale de Lausanne (EPFL), Lausanne, Switzerland
[37]Physik-Institut, Universität Zürich, Zürich, Switzerland
[38]Nikhef National Institute for Subatomic Physics, Amsterdam, The Netherlands
[39]Nikhef National Institute for Subatomic Physics and VU University Amsterdam, Amsterdam, The Netherlands
[40]NSC Kharkiv Institute of Physics and Technology (NSC KIPT), Kharkiv, Ukraine
[41]Institute for Nuclear Research of the National Academy of Sciences (KINR), Kyiv, Ukraine
[42]University of Birmingham, Birmingham, United Kingdom
[43]H.H. Wills Physics Laboratory, University of Bristol, Bristol, United Kingdom
[44]Cavendish Laboratory, University of Cambridge, Cambridge, United Kingdom
[45]Department of Physics, University of Warwick, Coventry, United Kingdom
[46]STFC Rutherford Appleton Laboratory, Didcot, United Kingdom
[47]School of Physics and Astronomy, University of Edinburgh, Edinburgh, United Kingdom
[48]School of Physics and Astronomy, University of Glasgow, Glasgow, United Kingdom
[49]Oliver Lodge Laboratory, University of Liverpool, Liverpool, United Kingdom
[50]Imperial College London, London, United Kingdom
[51]School of Physics and Astronomy, University of Manchester, Manchester, United Kingdom
[52]Department of Physics, University of Oxford, Oxford, United Kingdom
[53]Syracuse University, Syracuse, NY, United States
[54]Pontifícia Universidade Católica do Rio de Janeiro (PUC-Rio), Rio de Janeiro, Brazil
(associated with Institution Universidade Federal do Rio de Janeiro (UFRJ), Rio de Janeiro, Brazil)
[55]Institut für Physik, Universität Rostock, Rostock, Germany (associated with Institution Physikalisches Institut,
Ruprecht-Karls-Universität Heidelberg, Heidelberg, Germany)

[a]Also at P. N. Lebedev Physical Institute, Russian Academy of Science (LPI RAS), Moscow, Russia.

[b]Also at Università di Bari, Bari, Italy.

[c]Also at Università di Bologna, Bologna, Italy.

[d]Also at Università di Cagliari, Cagliari, Italy.

[e]Also at Università di Ferrara, Ferrara, Italy.

[f]Also at Università di Firenze, Firenze, Italy.

[g]Also at Università di Urbino, Urbino, Italy.

[h]Also at Università di Modena e Reggio Emilia, Modena, Italy.

[i]Also at Università di Genova, Genova, Italy.

[j]Also at Università di Milano Bicocca, Milano, Italy.

[k]Also at Università di Roma Tor Vergata, Roma, Italy.

[l]Also at Università di Roma La Sapienza, Roma, Italy.

[m]Also at Università della Basilicata, Potenza, Italy.

[n]Also at LIFAELS, La Salle, Universitat Ramon Llull, Barcelona, Spain.

[o]Also at Hanoi University of Science, Hanoi, Viet Nam.

[p]Also at Massachusetts Institute of Technology, Cambridge, MA, USA.